



Safe Feedback Motion Planning in Unknown Environments: An Instantaneous Local Control Barrier Function Approach

Cong Li¹ · Zengjie Zhang² · Nesrin Ahmed¹ · Qingchen Liu³ · Fangzhou Liu⁴ · Martin Buss¹

Received: 29 March 2023 / Accepted: 1 September 2023 / Published online: 14 October 2023
© The Author(s) 2023

Abstract

Mobile robots are desired with resilience to safely interact with prior-unknown environments and finally accomplish given tasks. This paper utilizes instantaneous local sensory data to stimulate the safe feedback motion planning (SFMP) strategy with adaptability to diverse prior-unknown environments without building a global map. This is achieved by the numerical optimization with the constraints, referred to as instantaneous local control barrier functions (IL-CBFs) and goal-driven control Lyapunov functions (GD-CLFs), learned from perceptual signals. In particular, the IL-CBFs reflecting potential collisions and GD-CLFs encoding incrementally discovered subgoals are first online learned from local perceptual data. Then, the learned IL-CBFs are united with GD-CLFs in the context of quadratic programming (QP) to generate the safe feedback motion planning strategy. Rather importantly, an optimization over the admissible control space of IL-CBFs is conducted to enhance the solution feasibility of QP. The SFMP strategy is developed with theoretically guaranteed collision avoidance and convergence to destinations. Numerical simulations are conducted to reveal the effectiveness of the proposed SFMP strategy that drives mobile robots to safely reach the destination incrementally in diverse prior-unknown environments.

Keywords Safe feedback motion planning · Collision avoidance · Instantaneous local control barrier function · Goal-driven control lyapunov function

1 Introduction

The safe operation of mobile robots in prior-unknown environments is important in applications such as the search and rescue in dangerous environments [1]. The promising solution is the so-called feedback motion planning (FMP) strategy that uses feedback (realtime interaction with environments) to endow mobile robots with adaptability towards dynamically changing environments [2–4]. However, the safety (collision avoidance) problem is often ignored in current FMP related works [5–8], especially considering the prior-unknown environment scenario. Thereby, we propose a safe feedback motion planning (SFMP) strategy to realize safe execution in prior-unknown environments and accomplish given tasks. We exploit instantaneous local sensory data to stimulate computationally cheap SFMP strategies in prior-unknown environments; Rather than firstly conducting a computationally intensive mapping process and then

planning on the constructed map to offer a safe solution. Besides, the utilized instantaneous local sensory data endows the resulting SFMP strategies with flexibility towards diverse environments.

1.1 Related Works

The traditional solutions to the motion planning problem mainly include grid-based [9], sampling-based [10], and numerical optimization based [11] algorithms. Note that it is hard to offer a complete review due to the page limit. Thus, the authors pick up the representative works here. The solutions mentioned above cannot be easily applied to prior-unknown environments given the following two reasons. Firstly, the effectiveness and performance of the above mentioned methods [9–11] rely on a pre-built perfect map. This is unavailable for the (partially) unknown environment scenario. Secondly, the open-loop motion planning strategies (a function of initial states only) in the works [9–11] are not competent to adapt to varying environments, or even small deviations from the expectations in practical applications. Departing from the mechanism of the above traditional

✉ Zengjie Zhang
z.zhang3@tue.nl

Extended author information available on the last page of the article

solutions, we utilize realtime interaction with environments to stimulate FMP strategies with resilience towards prior-unknown environments.

To further operate safely in prior-unknown environments, the mobile robot needs to discover and react to potential collisions. Rather than using the common collision avoidance tools such as artificial potential method [12], collision cone [13], navigation function [14], funnel [3, 4], and reachable set [15], we prefer to use the mechanism of control barrier function (CBF) [16] to facilitate the SFMP strategy given its simplicity (easier collision check) and rigorousness (theoretical guarantee of safety). Normally, CBFs are constructed using obstacle information such as location, shape, and number [16]. However, complete knowledge of obstacles in an unstructured environment is usually unavailable. Thus, the online learning of obstacle related CBFs is required if practitioners want to use CBFs to enforce safety in prior-unknown environments. The neural network parameterized CBFs are learned using a cost function that characterizes essential properties of CBFs [17–19]. The offline learning of barrier functions using expert demonstrations is adopted in [20, 21]. Besides, the CBF learning is formulated as a classification problem in [22], wherein a complete obstacle boundary is identified via the support vector machine method. The CBF learning problem is solved through a global perspective in the works [17–22] mentioned above. Alternatively, we attempt to learn CBFs from a local perspective in favour of computation efficiency. The resulting instantaneous local control barrier functions (IL-CBFs) are robust to previously-unobserved environments. Along with the safety problem discussed above, the reaching task to a predetermined goal position can be realized by control Lyapunov function (CLF) based analytical or numerical solutions [23] that are favored with theoretical convergence guarantees to target positions. However, either predetermined [23] or learned [24] CLF based solutions are inefficient to complete long-horizon tasks in practice. We solve this problem through a divide-and-conquer approach by discovering subgoals incrementally using sensory data and further constructing associated goal-driven control Lyapunov functions (GD-CLFs) for each subtask.

CBFs are often used with CLFs under a quadratic programming (QP) optimization [25]. However, the resulting QP is susceptible to infeasibility; especially considering limited motion commands. This gap has been marginally considered in existing works. A promising work [26] improves the QP feasibility by using the developed penalty and parameterization methods. Besides, control-sharing CBFs [27] and control-sharing CLFs [28] are investigated separately to improve the QP feasibility within consideration of multiple CBF or CLF constraints. However, the theoretically promising conclusions in [27, 28] no longer hold when CBFs and CLFs are used together. This work enhances the QP

feasibility by enlarging the admissible control spaces (ACSs) of the IL-CBF constraints via our formulated linear programming (LP) optimization, and introducing a relaxation variable for the GD-CLF constraints similar to [29].

1.2 Contributions

The main contribution of this paper is learning IL-CBFs and GD-CLFs from sensory data to encode safety and task requirements, respectively. These online learned constraints considered in the QP optimization process allow us to analyze and fulfill requirements of safety and task (convergence to goal positions). Another contribution is conducting an optimization over the ACSs of IL-CBF constraints to enhance the solution feasibility of the associated QP. The feasibility of QP under multiple constraints remains an open problem [26]. Towards this end, we reinvestigate the learned IL-CBF constraints in a motion control space (the axis is the motion command). This allows us to design a metric to quantify the volume of the ACS of the IL-CBF and further enlarge its area under an LP optimization process.

The remainder of this paper is organized as follows. Section 2 presents the problem formulation. Then, the IL-CBF and GD-CLF learning processes are clarified in Sections 3 and 4, respectively. Thereafter, the learned IL-CBFs and GD-CLFs are united through the QP in Section 5, and the strategy to enhance the QP feasibility is shown in Section 6. The SFMP strategy is numerically validated in Section 7. Finally, the conclusion is shown in Section 8.

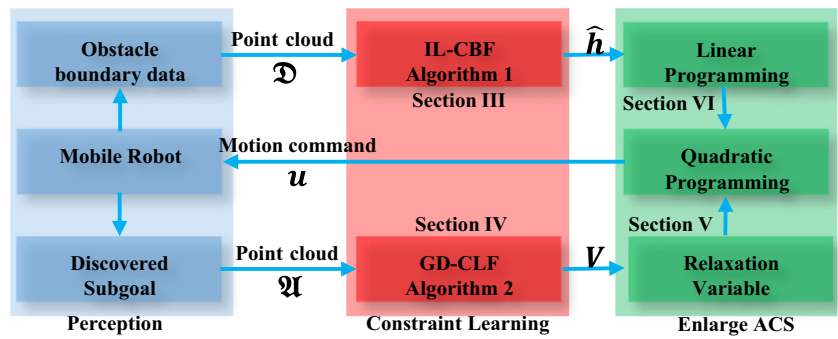
Notations: Throughout this paper, \mathbb{R} , \mathbb{R}^+ , and \mathbb{R}_0^+ denote the set of real, positive, and non-negative real numbers, respectively; \mathbb{N}^+ denotes the set of non-negative integers; \mathbb{R}^n is the Euclidean space of n -dimensional real vector; $\mathbb{R}^{n \times m}$ is the Euclidean space of $n \times m$ real matrices; The i -th entry of a vector $x = [x_1, \dots, x_n]^T \in \mathbb{R}^n$ is denoted by x_i , and $\|x\| = \sqrt{\sum_{i=1}^n |x_i|^2}$ is the Euclidean norm of the vector x ; The ij -th entry of a matrix $D \in \mathbb{R}^{n \times m}$ is denoted by d_{ij} , and $\|D\| = \sqrt{\sum_{i=1}^n \sum_{j=1}^m |d_{ij}|^2}$ is the Frobenius norm of the matrix D . For notational brevity, time dependence is suppressed without causing ambiguity.

2 Problem Formulation

This work investigates the safe operation problem of a mobile robot in previously unforeseen environments. We model the investigated mobile robot as:

$$\begin{bmatrix} \dot{p} \\ \dot{v} \end{bmatrix} = \begin{bmatrix} 0_{2 \times 2} & I_{2 \times 2} \\ 0_{2 \times 2} & 0_{2 \times 2} \end{bmatrix} \begin{bmatrix} p \\ v \end{bmatrix} + \begin{bmatrix} 0_{2 \times 2} \\ I_{2 \times 2} \end{bmatrix} u, \quad (1)$$

Fig. 1 Schematic of the SFMP strategy that maps raw sensory data to motion commands. The IL-CBFs learned from sensory data in Section 3 characterize the obstacle boundaries; The decomposed short-horizon subtasks are encoded by GD-CLFs clarified in Section 4; The LP optimization is conducted to enlarge the ACSs in Section 6 to improve the feasibility of the QP formulated in Section 5



where $p := [x, y]^T$, $v := [v_x, v_y]^T$, and $u := [u_x, u_y]^T \in \mathbb{R}^2$ are the positions, velocities, and motion commands, respectively. For simplicity, we assume that the robot localization is perfect, i.e., the accurate vehicle state is available¹.

Assume that there exist multiple prior unknown obstacles \mathcal{O}_l in an environment \mathcal{E} , where $l \in \mathcal{L} := \{l | l = 1, 2, \dots, L\}$ and $L \in \mathbb{N}^+$ is an uncertain value. The objective is to design an SFMP strategy u to drive the mobile robot Eq. 1 to operate safely in a prior-unknown environment \mathcal{E} and finally reach the predetermined target position $p_d := [x_d, y_d]^T \in \mathbb{R}^2$. We formulate the safe operation problem mentioned above as a constrained optimization problem stated as:

$$\min_u J := \int_{t_0}^{t_f} u^T u dt \tag{2a}$$

s.t. Eq. 1

$$p(t_0) = p_0; v(t_0) = v_0 \tag{2b}$$

$$u(t) \in \mathcal{U}, \forall t \in [t_0, t_f] \tag{2c}$$

$$p(t) \cap \bigcup_{l=1}^L \mathcal{O}_l = \emptyset, \forall t \in [t_0, t_f] \tag{2d}$$

$$\|p(t_f) - p_d\| \leq \delta, \tag{2e}$$

where the kinodynamic constraint Eq. 1 and the bounded input space $\mathcal{U} \subseteq \mathbb{R}^2$ in Eq. 2c are considered to ensure the resulting SFMP strategy obeying the physical feasibility. A prior set threshold $\delta \in \mathbb{R}^+$ in Eq. 2e is used to check whether the reach task is completed. A quadratic energy function is adopted in Eq. 2a to reflect designers' preference for the energy minimization.

The aforementioned safe operation problem Eq. 2 is nontrivial given the constraints indicating different (might conflicting) objectives of safety and performance maximization; and the requirement of constraint satisfaction under uncertainty (limited knowledge of the environment \mathcal{E}). This work develops an SFMP strategy to solve Eq. 2, whose mechanism is illustrated in Fig. 1. In particular, we use perception

inputs to learn IL-CBFs and GD-CLFs that are utilized to achieve collision avoidance and accomplish given tasks.

3 IL-CBF Online Learning

This section elucidates the mechanism of learning IL-CBFs from sensory data. In particular, the detected local obstacle information is utilized to learn local barrier functions to describe the partial obstacle boundaries; and the learned local barrier functions update along with continuously coming data to tackle the prior-unknown environment. Our developed IL-CBFs are employed to formulate the QP problem in Section 5 to conduct collision avoidance with prior-unforeseen obstacles.

As illustrated in Fig. 2, the whole boundaries of the obstacles \mathcal{O}_l in \mathcal{E} could be described by the barrier functions $h_l(p) \in \mathbb{R}$ using the complete knowledge of obstacles [16], which is however unavailable in our investigated problem Eq. 2. Thus, the explicit forms of $h_l(p)$ that characterize the

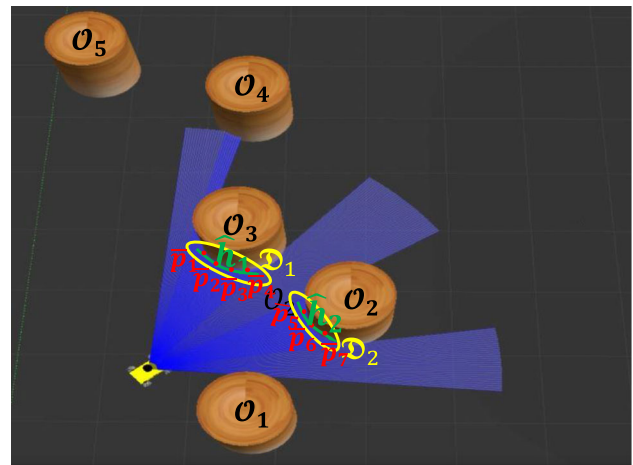


Fig. 2 Graphical illustration of IL-CBFs and obstacles. The whole boundaries of obstacles \mathcal{O}_l are described by explicit CBFs $h_l = (x - x_{o_l})^2 + (y - y_{o_l})^2 - r_l^2$, $c_l = (x_{o_l}, y_{o_l})$, $l = 1, 2, 3, 4, 5$. The mobile robot observes $\mathcal{D} = \{\bar{p}_1, \bar{p}_2, \dots, \bar{p}_7\}$ and classifies \mathcal{D} into subgroups \mathcal{D}_k , $k = 1, 2$. Thus, $K = 2$, and $I_1 = 4$, $I_2 = 3$ here. The mobile robot learns \hat{h}_k based on the k -th data subgroup \mathcal{D}_k

¹ The localization is realizable by the low-cost dead reckoning method. Dealing with its cumulative error is a different research direction, which is beyond the scope of this paper.

dangerous regions \mathcal{O}_l are unavailable. We observe in Fig. 2 that only partial obstacle boundaries of \mathcal{O}_l pose threats to the mobile robot safety at a certain period. This motivates us to utilize the local sensory data to learn the local barrier functions, corresponding to the partial obstacle boundary within the mobile robot’s sensor horizon, to address the collision avoidance problem.

Assume that the mobile robot is embedded with a sensor with a restricted angle S_θ and a limited horizon S_r . The value of S_θ is given, and the value of S_r satisfies

$$S_r \geq D_{\text{brake}} := \|v_{\text{max}}\|^2 / \|a_{\text{max}}\|, \tag{3}$$

where $v_{\text{max}}, a_{\text{max}} \in \mathbb{R}^2$ are the maximum velocity and breaking acceleration of the mobile robot Eq. 1. Here D_{brake} denotes the travelled distance when the mobile robot in the maximum velocity brakes using the maximum breaking acceleration.

Remark 1 *The setting of the sensor horizon S_r in Eq. 3 is beneficial to the emergence case where our developed SFMP strategy fails to guarantee safety. In this scenario, the mobile robot brakes to avoid collisions.*

The sensor provides a point cloud \mathcal{L} . We term $\mathcal{D} := \{\bar{p}_1, \bar{p}_2, \dots\} \subset \mathcal{L}$ as the data group of the sensed obstacle boundaries, wherein $\bar{p}_i := [\bar{x}_i, \bar{y}_i]^\top \in \mathbb{R}^2$ is the position of the i -th detected obstacle boundary point. In an environment \mathcal{E} with densely populated obstacles, data points in \mathcal{D} might concern multiple isolated obstacles, as displayed in Fig. 2. Therefore, we adopt the robust clustering algorithm—density-based spatial clustering of applications with noise (DBSCAN) [30]—to cluster \mathcal{D} into multiple subgroups $\mathcal{D}_k := \{\bar{p}_{k_1}, \bar{p}_{k_2}, \dots\}$, wherein $\bar{p}_{k_i} := [\bar{x}_{k_i}, \bar{y}_{k_i}]^\top \in \mathbb{R}^2$ denotes the i -th data point of the k -th data subgroup $\mathcal{D}_k, i \in \mathcal{I} := \{i | i = 1, \dots, I_k\}$ with $I_k \in \mathbb{N}^+$ being the total number of data points in the \mathcal{D}_k , and $k \in \mathcal{K} := \{k | k = 1, \dots, K\}$ with $K \in \mathbb{N}^+$ being the sum of the local obstacle boundary considered in the current period.

Remark 2 *The DBSCAN algorithm is compatible with our IL-CBF learning process given that it could determine the number of to be learned IL-CBFs (i.e., the values of K) automatically without using prior knowledge of environments.*

In the following, we clarify the mechanism of the IL-CBF learning focusing on the k -th data subgroup \mathcal{D}_k . Assume that i -th data pair \bar{p}_{k_i} satisfies

$$\bar{y}_{k_i} = \mathcal{F}(\bar{x}_{k_i}, \zeta_k) + \varepsilon_k, \quad k \in \mathcal{K}, \tag{4}$$

where $\mathcal{F}(\bar{x}_{k_i}, \zeta_k) \in \mathbb{R}$ is one n -th degree polynomial function with a parameter $\zeta_k \in \mathbb{R}^{n+1}$ to be learned; and $\varepsilon_k \sim N(0, \sigma^2)$ denotes an assumed Gaussian sensor noise with a zero mean and a constant variance $\sigma \in \mathbb{R}$.

Algorithm 1 IL-CBF online learning algorithm

Input: Point cloud \mathcal{D} ;
Output: $\hat{h}_k, k = 1, \dots, K$;
 1: $K = \text{DBSCAN}(\mathcal{D})$ ▷ Robust clustering
 2: **for** $k = 1 : K$ **do**
 3: $\hat{\zeta}_k = \text{M-estimate}(\mathcal{D}_k)$ Eq. 6 ▷ Robust regression
 4: $\hat{h}_k = y - \mathcal{F}(x, \hat{\zeta}_k)$ Eq. 7
 5: **end for**

Remark 3 *There exist multiple choices for \mathcal{F} , such as Gaussian models, linear fitting, and rational polynomials [31]. Considering the generality and simplicity issues, a polynomial model is chosen here.*

Based on Eq. 4 and the point cloud \mathcal{D}_k from the sensor, ζ_k is learned to minimize the approximation error

$$\hat{\zeta}_k = \arg \min_{\zeta_k} \sum_{i=1}^{I_k} (\bar{y}_{k_i} - \mathcal{F}(\bar{x}_{k_i}, \zeta_k))^2, \quad k \in \mathcal{K}. \tag{5}$$

To address potential noises and outliers that exist in the measurement data, the robust regression technique— M -estimate [32]—is adopted here. By using the M -estimate, the learning of ζ_k in Eq. 5 is rewritten as

$$\hat{\zeta}_k = \arg \min_{\zeta_k} \sum_{i=1}^{I_k} \rho \left(\frac{\bar{y}_{k_i} - \mathcal{F}(\bar{x}_{k_i}, \zeta_k)}{\gamma} \right), \quad k \in \mathcal{K}, \tag{6}$$

where $\rho(r) = c^2 / (1 - (1 - (r/c)^2)^3)$ is a robust loss function with $c = 1.345$; γ is a scale parameter estimated as $\gamma = 1.48 [\text{med}_i |(\bar{y}_{k_i} - \mathcal{F}(\bar{x}_{k_i}, \zeta_{k_0}) - \text{med}_i(\bar{y}_{k_i} - \mathcal{F}(\bar{x}_{k_i}, \zeta_{k_0}))|]$ with ζ_{k_0} being the initial value of ζ_k . More details about the M -estimate approach are referred to [32].

Using the learned $\hat{\zeta}_k$ Eq. 6, we construct the IL-CBF \hat{h}_k as

$$\hat{h}_k = y - \mathcal{F}(x, \hat{\zeta}_k), \quad k \in \mathcal{K}, \tag{7}$$

which is a valid CBF according to [16, Definition 5].

The IL-CBF learning process mentioned above is summarized in Algorithm 1. The mobile robot uses Algorithm 1 to update the learned IL-CBFs continuously based on the newly observed sensory data during the operation process. The IL-CBF learning is favored with computation simplicity. Thus, it is practical to update the learned IL-CBFs at each step, which is favourable for the mobile robot to observe the environmental changes in time and make corresponding reactions.

Remark 4 *Alternatively, we are able to realize the CBF learning in an incremental way along with a steady stream of data, i.e., attempting to gradually learn one global barrier function that describes the whole obstacle boundary. However,*

Algorithm 2 GD-CLF online learning algorithm

Input: Point cloud $\mathfrak{A} := \{\tilde{p}_1, \tilde{p}_2, \dots\}$; Robot position p .

Output: \tilde{p}_{d_j} , and $V_j, j = 1, \dots, J$;

1: $\tilde{p}_{d_1} = \arg \min_{\tilde{p}_i \in \mathfrak{A}} \|\tilde{p}_i - p_d\|$ and get V_1 Eq. 8

2: **if** $\|p - \tilde{p}_{d_j}\| \leq \delta$ **then**

3: $\tilde{p}_{d_j} = \arg \min_{\tilde{p}_i \in \mathfrak{A}} \|\tilde{p}_i - p_d\|$

4: $j = j + 1$ and update V_j Eq. 8

5: **end if**

we found in practice that this increment learning approach shows no obvious advantage in terms of collision avoidance but introduces additional computation loads. Thus, we forgo using all detected data to gradually build a perfect map, rather than only using instantaneous local sensory information.

Remark 5 The clarified IL-CBF learning in this section is especially compatible with low-end sensors that only provide low-dimensional data. The limited data, however, is not enough to build a global map or describe the whole obstacle boundary.

4 GD-CLF Automatic Construction

The data group \mathfrak{D} concerning the detected obstacle boundaries is utilized in Section 3 to facilitate collision avoidance in prior-unknown environments. This section exploits the remaining local collision-free sensory data group $\mathfrak{A} := \mathcal{L} \ominus \mathfrak{D}$ to complete the long-horizon task. Specifically, we first utilize the data group \mathfrak{A} to discover subgoals using an Euclidean distance metric. Then, we construct the associated GD-CLF for each subtask (subgoal). The automatically constructed GD-CLFs serve as constraints of the QP optimization in Section 5, whose solution ensures that the mobile robot travels toward the discovered subgoals incrementally and finally reaches the destination.

Normally, the common CLF used in [23, 24] is inefficient to account for a long-horizon goal. Thus, through a divide-and-conquer perspective, we use sensory data \mathfrak{A} to discover the subgoals $\tilde{p}_{d_j} := [x_{d_j}, y_{d_j}]^T \in \mathbb{R}^2, j \in \mathcal{J} := \{j | j = 1, \dots, J\}$ with $J \in \mathbb{N}^+$, based on a Euclidean distance metric (line 3 of Algorithm 2). In particular, we choose the nearest collision-free waypoint (\tilde{p}_4 in Fig. 3 for example) toward the goal position p_d as the next subgoal (\tilde{p}_{d_1} in Fig. 3 for example). The automatically determined intermediate waypoints \tilde{p}_{d_j} would forwardly progress toward the final desired position p_d .

The automatically determined subgoals \tilde{p}_{d_j} from Algorithm 2 divide the long-horizon task into J short-horizon subtasks. For each subtask, we construct the GD-CLF :

$$V_j = (p - \tilde{p}_{d_j})^T P (p - \tilde{p}_{d_j}) + (v - v_{d_j})^T Q (v - v_{d_j}), j \in \mathcal{J} \tag{8}$$

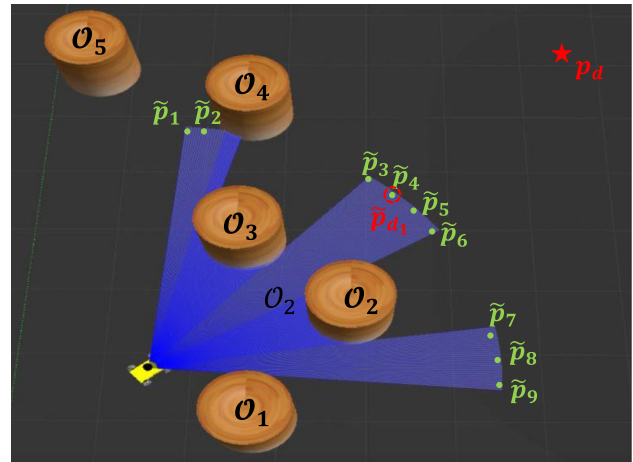


Fig. 3 Graphical illustration of GD-CLFs and subgoals. The mobile robot uses the collision-free data group $\mathfrak{A} = \{\tilde{p}_1, \tilde{p}_2, \dots, \tilde{p}_9\}$ and Algorithm 2 to determine the position $\tilde{p}_4 \in \mathfrak{A}$ as its first subgoal \tilde{p}_{d_1} . Then, the constructed GD-CLF V_1 guides the robot toward \tilde{p}_{d_1} . The robot would determine its $j + 1$ -th subgoal when it arrives at δ -neighbourhood around the j -th subgoal. Following the above-mentioned process, the mobile robot would travel along the successively discovered subgoals $\tilde{p}_{d_2}, \tilde{p}_{d_3}, \dots$, and finally reaches the goal p_d

where $P, Q \in \mathbb{R}^{2 \times 2}$ are predetermined positive definite matrices; and $v_{d_j} \in \mathbb{R}^2$ could be a zero or a prior-given constant velocity vector. The constructed GD-CLF V_j Eq. 8 updates as the subgoal \tilde{p}_{d_j} refreshes using Algorithm 2.

Remark 6 Note that we construct IL-CBFs Eq. 7 in Section 3 and GD-CLFs Eq. 8 in Section 4 assuming that $\mathcal{U} = \mathbb{R}^2$ for convenience, i.e., the influence of input saturation is ignored temporarily. This problem is later tackled in Section 6 by explicitly analysing the potential conflicts between IL-CBF, GD-CLF, and input constraints.

5 Safe Feedback Motion Planning Strategy

This section incorporates the learned IL-CBFs Eq. 7 and the constructed GD-CLFs Eq. 8 in a QP optimization to generate the SFMP strategy that drives the mobile robot to safely reach the target position incrementally.

By dividing the period $[t_0, t_f]$ into multiple intervals $[t_0 + mT, t_0 + (m + 1)T]$ [26], where $m \in \mathbb{N}^+$, and $T \in \mathbb{R}^+$ is the sampling time, we reformulate the original safe operation problem Eq. 2 into a sequence of QPs at each interval:

$$\min_{u,v} u(t)^T u(t) + \bar{c}_1 v^2(t) \tag{9a}$$

s.t. Eqs. 1, 2b, 2c

$$\ddot{h}_k + \alpha_{k_1} \dot{h}_k + \alpha_{k_2} h_k \geq 0, \tag{9b}$$

$$\dot{V}_j + \bar{c}_2 V_j \leq v, \tag{9c}$$

where $v(t) \in \mathbb{R}$ is a relaxation variable to relax the GD-CLF constraint to improve the QP feasibility [29]; $\alpha_{k_1}, \alpha_{k_2}, \bar{c}_1, \bar{c}_2 \in \mathbb{R}$ are parameters to be determined. The reformulated QP problem Eq. 9 unifies the safety requirements Eqs. 2c and 9b, the task requirements Eq. 9c, and the optimization over energy Eq. 9a to generate a multi-objective SFMP strategy that drives the mobile robot to progressively reach subgoals while avoiding obstacles. Note that our developed SFMP strategy from Eq. 9 only requires the information of the mobile robot position p and the target position p_d to solve the safe operation problem Eq. 2 in prior-unknown environments.

Remark 7 Although the proposed SFMP strategy Eq. 9 is restricted to the mobile robots following a second-integrator-type kinematics Eq. 1, it could be easily extended to the mobile robots following an unicycle-type kinematics according to the method proposed in [33]. Besides, the specific cost function Eq. 9a in a quadratic input form is utilized for efficient computation concerns. This is especially worthwhile for low-cost platforms with limited computational resources. The online learned IL-CBFs Eq. 9b and the automatically constructed GD-CLFs Eq. 9c are not restricted to specific sensors. The required data could be provided by different sensors such as LiDAR or cameras.

6 Optimized Admissible Control Space

The potential conflicts between constraints Eqs. 2c, 9b, and 9c might result in the infeasibility problem of the QP Eq. 9 formulated in Section 5. This section formulates an optimization over the ACS of the IL-CBF associated constraint Eq. 9b to enhance the solution feasibility of QP.

Denoting the ACSs for constraints Eqs. 9b and 9c as $\mathcal{A}_1 := \{u \in \mathbb{R}^2 | \ddot{h}_k + \alpha_{k_1} \dot{h}_k + \alpha_{k_2} h_k \geq 0, k \in \mathcal{K}\}$, and $\mathcal{A}_2 := \{u \in \mathbb{R}^2 | \dot{V}_j + c_2 V_j \leq v\}$, respectively. Thereby, the shared control space concerning constraints Eqs. 2c, 9b, and 9c is termed as $\mathcal{S} = \mathcal{A}_1 \cap \mathcal{A}_2 \cap \mathcal{U}$. It is desirable that $\mathcal{S} \neq \emptyset$ always holds, i.e., the feasibility of the QP problem is always guaranteed. This is a nontrivial problem; especially multiple constraints are considered. Improving the possibility of satisfying $\mathcal{S} \neq \emptyset$ is equivalent to enlarging the volume of \mathcal{S} . Given that the relationship between sets \mathcal{A}_1 and \mathcal{A}_2 is hard to be described and the volume of \mathcal{U} is predetermined, we could transform the enlargement of the volume of \mathcal{S} into the enlargement of the volumes of ACSs \mathcal{A}_1 and \mathcal{A}_2 independently. A relaxation variable v has been used in Eq. 9c to enlarge the volume of \mathcal{A}_2 . In the following, we attempt to enlarge the volume of the ACS \mathcal{A}_1 to improve the feasibility of the QP problem Eq. 9. In particular, we firstly seek for a criterion for the volume of the ACS \mathcal{A}_1 in Section 6.1 by investigating the relationship between sets \mathcal{A}_1 and \mathcal{U} . Then,

an LP optimization problem is formulated in Section 6.2 to optimize the above volume criterion to enlarge the volume of the ACS \mathcal{A}_1 .

6.1 Criterion of ACS

The enlargement of the ACS \mathcal{A}_1 is equivalent to enlarge each IL-CBF \hat{h}_k associated ACS that is denoted as $\mathcal{A}_{1_k} := \{u \in \mathbb{R}^2 | \ddot{h}_k + \alpha_{k_1} \dot{h}_k + \alpha_{k_2} h_k \geq 0\}, k \in \mathcal{K}$. The explicit form of the learned k -th IL-CBF follows $\hat{h}_k = y - \hat{\zeta}_k^\top \Phi$, where $\Phi := [1, x, x^2, \dots, x^n]$. We substitute the explicit \hat{h}_k into Eq. 9b and rewrite the inequality as

$$Au_x + u_y + a_k^\top \Psi > 0, \tag{10}$$

where $A := \hat{\zeta}_k^\top \frac{\partial \Phi}{\partial x} \in \mathbb{R}, \alpha_k = [\alpha_{k_1}, \alpha_{k_2}]^\top \in \mathbb{R}^2, \Psi := [\hat{\zeta}_k^\top \frac{\partial \Phi}{\partial x} v_x - v_y, \hat{\zeta}_k^\top \frac{\partial^2 \Phi}{\partial x^2} v_x^2 + \hat{\zeta}_k^\top \Psi - y]^\top \in \mathbb{R}^2$.

Based on the reformulated Eq. 10, the geometric interpretations of the ACS \mathcal{A}_{1_k} as well as the limited motion command set \mathcal{U} are depicted in Fig. 4. We found that a smaller value of $a_k^\top \Psi$ implies a larger area of the ACS \mathcal{A}_{1_k} . Thus, it is reasonable to choose the value of $a_k^\top \Psi$ as a metric to quantify the volume of the ACS \mathcal{A}_{1_k} , which is optimized in the subsequent subsection.

6.2 Optimization of ACS

This subsection clarifies the optimization over the metric $a_k^\top \Psi$, which is formulated as a LP optimization problem

$$\min_{\alpha_k} \alpha_k^\top \Psi \tag{11a}$$

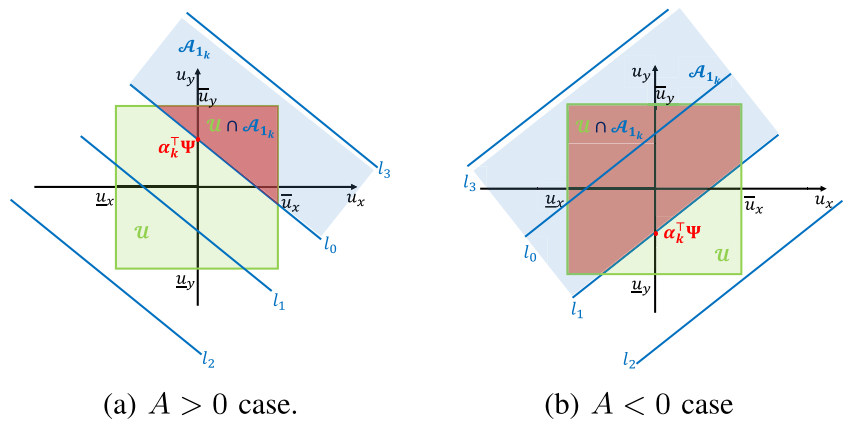
$$\text{s.t. } 0 < \alpha_{k_1}, \alpha_{k_2} < \bar{\alpha}_k \tag{11b}$$

$$a_{k_1}^2 - 4\alpha_{k_2} \geq 0 \tag{11c}$$

where $\bar{\alpha}_k \in \mathbb{R}^+$ is the predetermined bound for the optimization variable. The formulated LP Eq. 11 is solved by the off-the-self *fmincon* solver. The core idea of the above LP is to select suitable values of α_{k_1} and α_{k_2} to minimize $\alpha_k^\top \Psi$ while respecting constraints Eqs. 11b and 11c. A decreased $\alpha_k^\top \Psi$ leads to a enlarged \mathcal{A}_{1_k} . Thereby, the QP feasibility is improved.

Remark 8 The constraints Eqs. 11b and 11c are the simplification of the following three constraints: (1) $a_{k_1}^2 - 4\alpha_{k_2} \geq 0$; (2) $\frac{-\alpha_{k_1} + \sqrt{a_{k_1}^2 - 4\alpha_{k_2}}}{2} < 0$; (3) $\frac{-\alpha_{k_1} - \sqrt{a_{k_1}^2 - 4\alpha_{k_2}}}{2} < 0$. These three constraints ensure that the roots of Eq. 9b's related polynomials $\mathcal{P}(\lambda) = \lambda^2 + \alpha_{k_1} \lambda + \alpha_{k_2}$ are all negative. These constraints ensure that the optimized parameter α_k^* leads to valid HO-CBFs. More details about HO-CBFs are referred to [27].

Fig. 4 The geometric interpretation of the sets \mathcal{A}_{1_k} (the blue shaded area) and \mathcal{U} (the green shaded area). Here $l_k = Au_x + u_y + \alpha_k^T \Psi = 0$. The comparison of the volume of \mathcal{A}_{1_k} follows $\mathcal{A}_{1_k}^{l_2} > \mathcal{A}_{1_k}^{l_1} > \mathcal{A}_{1_k}^{l_0} > \mathcal{A}_{1_k}^{l_3}$ for both two cases. For the l_3 case, $\mathcal{A}_{1_k} \cap \mathcal{U} = \emptyset$, i.e., there is no feasible motion command to ensure safety



7 Numerical Simulation

This section conducts numerical simulations to validate the efficiency of our proposed SFMP strategy Eq. 9. In particular, Section 7.1 focuses on a reach-avoid benchmark problem to validate the effectiveness of the LP optimization Eq. 11. The resulting enlarged ACS leads to better performance. Then, we validate the efficiency of the SFMP strategy under two representative environments: an obstacle-filled outdoor scenario in Section 7.2, and a maze indoor scenario in Section 7.3. The mobile robot safely operates in the unforeseen outdoor or the maze indoor environment and completes the given long-horizon reach task using the SFMP strategy, generated by solving the QP Eq. 9 within consideration of our developed IL-CBF Eq. 7 and GD-CLF Eq. 8. The QP feasibility is preserved during the operation process via the LP optimization Eq. 11.

Furthermore, the effectiveness of our proposed SFMP strategy is validated based on the constructed high-fidelity simulator in Section 7.4, wherein the repeated validations in one large environment and the comparison with one baseline are considered.

7.1 Validation of Optimized ACS

This subsection validates the effectiveness of our developed optimized ACS strategy Eq. 11 clarified in Section 6.2 based on a benchmark reach-avoid task. A mobile robot modelled

as Eq. 1 is desired to move from an initial position p_0 to a desired position p_d while avoiding one circle obstacle \mathcal{O} (centered at $c = (1, 1)$ and with radius $r = 1$) during the operation process, as illustrated in Fig. 5a. The detailed simulation settings are referred to in Table 1. Note that to avoid IL-CBFs and GD-CLFs' influence on the QP feasibility, this subsection uses a prior-known CBF to achieve collision avoidance, and an assumed nominal motion planning strategy to accomplish the reaching task with desired performance.

We formulate the QP optimization problem as

$$\min_u \|u - u_n\|^2 \tag{12a}$$

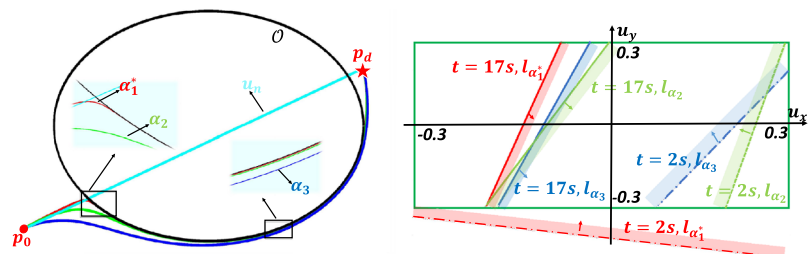
$$\text{s.t. } -0.3 < u_x, u_y < 0.3 \tag{12b}$$

$$\dot{h} + \alpha_1^* \dot{h} + \alpha_2^* h \geq 0, \tag{12c}$$

to solve the reach-avoid task mentioned above, where α_1^* and α_2^* are the optimized variables after solving the LP Eq. 11 based on the known CBF h presented in Table 1. For comparison, prior-chosen constant vectors $\alpha_2 = [4, 1]^T$, $\alpha_3 = [4, 2]^T$ are picked to construct the constraint Eq. 12c. Note that the feasibility of the QP Eq. 12 is easily lost without choosing the suitable values of α required for the HO-CBF. Here α_2 and α_3 are well-debugged parameters to ensure the QP feasibility.

As displayed in Fig. 5a, the nominal u_n is an unsafe motion command given that the mobile robot driven by the u_n crosses

Fig. 5 The performance comparison between the optimized α_1^* and the predetermined α_2, α_3 associated QP solutions



(a) The comparison regarding $p(t)$. (b) The comparison regarding ACS.

Table 1 The parameter settings of the reach-avoid task

Initial values	$p_0 = [-0.2, 0.1]^T, v_0 = [0, 0]^T, T = 10 \text{ Hz}$
Target values	$p_d = [2, 1.5]^T, v_d = [0, 0]^T$
CBF	$h = (x - 1)^2 + (y - 1)^2 - 1$
Nominal policy	$u_n = -0.2(p - p_d) - 0.9(v - v_d)$
QP and LP	$\bar{u}_x, \bar{u}_y = 0.3, \alpha_1(t_0) = [5, 6]^T, \bar{\alpha}_1 = 7$

the obstacle \mathcal{O} . The minimally corrected u_n by solving the QP Eq. 12 drives the mobile robot to safely reach the destination. Furthermore, as shown in Fig. 5a, the trajectory of the optimized α_1^* case is closer to the desired trajectory (the cyan line) associated with u_n as a consequence of the enlarged ACS. The ACSs of the constraint Eq. 12c at $t = 2s$ and $t = 17s$ are displayed in Fig. 5b. It is shown that the α_1^* 's associated ACS is larger than the related ones of α_2 and α_3 . This validates the effectiveness of the LP optimization Eq. 11.

7.2 Validation in Outdoor Scenario

This subsection validates the efficiency of our proposed SFMP strategy Eq. 9 in an obstacle densely cluttered environment (see Fig. 6). The numerical simulation is conducted on the basis of the Mobile Robotics Simulation Toolbox [34] and the quadprog solver of the Optimization Toolbox [35]. The detailed parameter settings to solve the formulated QP Eq. 9 and LP Eq. 11 are presented in Table 2.

It is shown in Fig. 6a–c that the mobile robot exploits sensed obstacle boundary data to learn the IL-CBFs \hat{h}_1, \hat{h}_2 using Algorithm 1, and uses collision-free data to discover the subgoals $\tilde{p}_{d_1}, \tilde{p}_{d_2}$ via Algorithm 2. As displayed in Fig. 6d, the mobile robot safely reaches the subgoals $\tilde{p}_{d_1}, \tilde{p}_{d_2}$ sequentially and finally reach the destination p_d (same with \tilde{p}_{d_3}). Thus, it is concluded that the learned IL-CBFs Eq. 7 ensure collision avoidance with unforeseen obstacles, and the constructed GD-CLFs Eq. 8 based on the discovered subgoals guarantee the task fulfillment. The evolution trajectories of the motion command u , and the optimized parameter α^* are displayed in Fig. 7a and b, respectively. The input saturation is satisfied, and the LP Eq. 11 outputs the optimized α^* to ensure the feasibility of the QP Eq. 9 during the whole oper-

ation process. A supplemental video for the outdoor scenario is referred to in <https://youtu.be/FZsNc0UzEVs>.

7.3 Validation in Indoor Scenario

This subsection further validates the effectiveness of our designed SFMP strategy Eq. 9 in a maze simulation environment (see Fig. 8). It is worth mentioning that the application of common CBFs in a maze environment is seldom found in existing works. This is because multiple typical CBFs are required to achieve collision avoidance in such a maze environment, and certain CBFs would unavoidably treat collision-free spaces as unsafe regions. In this case, the mobile robot behaves conservatively and the QP might lose its feasibility. In particular, for the maze environment displayed in Fig. 8, it is nontrivial to design barrier functions to separate safe and unsafe regions even though we have the full knowledge of the environment. However, our developed IL-CBFs can efficiently deal with this maze environment. The detailed parameters to realize the safe operation in the maze environment are provided in Table 3. Accompanying simulation videos are available at <https://youtu.be/FZsNc0UzEVs>.

As displayed in Fig. 8, the mobile robot operates safely in the maze environment and finally reaches the goal position p_d . However, we observe inefficient operation (shown in the blue rectangle of Fig. 9a) of the mobile robot in this unforeseen maze environment. This is due to the simple heuristic (the shortest distance rule in particular) used in Algorithm 2. This problem could be avoided by changing the sensor range in an adaptive way. We deliberately present this incomplete case to show the potential drawback of our method. The trajectories of the mobile robot's velocity v , motion command u and optimized α^* are displayed in Fig. 9b, c, and d, respectively. The input saturation is always satisfied and α^* updates to ensure the QP feasibility.

Table 2 The parameter settings of the outdoor scenario

Initial values	$p_0 = [2, 4]^T, v_0 = [1, 1]^T, T = 10 \text{ Hz}$
Target values	$p_d = [10, 10]^T, v_d = [0, 0]^T$
IL-CBF	$\Phi = [1, x, x^2], S_\theta = [-\pi/2, \pi/2], S_r = 0.5 \text{ m}$
GD-CLF	$P = \begin{bmatrix} 25 & 12.5 \\ 12.5 & 25 \end{bmatrix}, Q = \begin{bmatrix} 50 & 25 \\ 25 & 50 \end{bmatrix}$
	$S_\theta = [-\pi, \pi], S_r = 4 \text{ m}, \bar{c}_2 = 1.5$
QP and LP	$\bar{u}_x, \bar{u}_y = 20, \bar{c}_1 = 1, \alpha(t_0) = [5, 6]^T, \bar{\alpha} = 6$

Fig. 6 The illustration of the robotic movement in the outdoor scenario. The black circles denote the prior-unknown obstacles; The dark green \hat{h}_1 and \hat{h}_2 denote the learned IL-CBFs; The light green \tilde{p}_{d_i} represents the discovered subgoal; The light green p_0 and the red p_d denote the initial and target positions, respectively

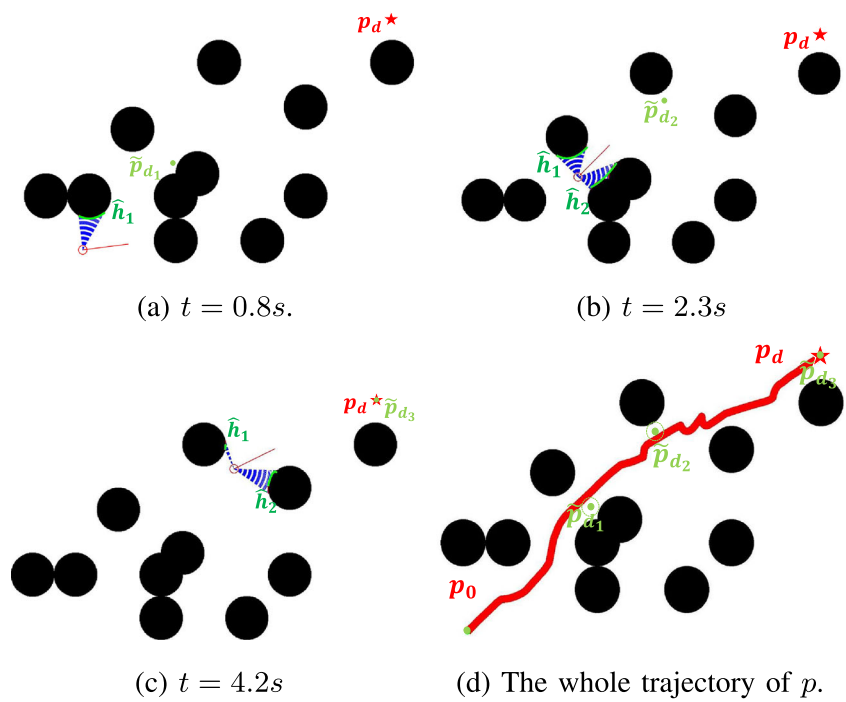


Fig. 7 The trajectories of u , and α^* for the outdoor scenario

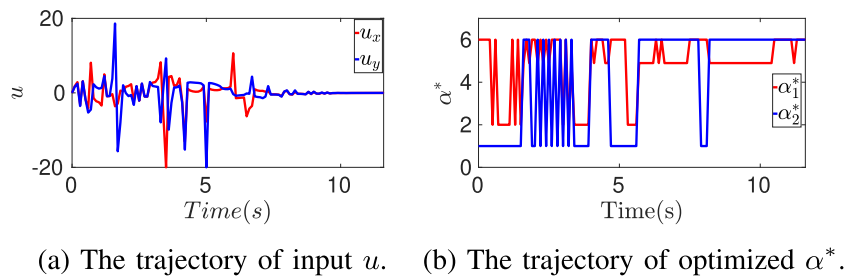


Fig. 8 The illustration of the robotic movement in the indoor scenario. The thick black lines represent walls; The dark green \hat{h}_i denotes the i -th learned IL-CBF; The light green \tilde{p}_{d_i} represents the discovered i -th subgoal; The light green p_0 and the red p_d denote the initial and target

positions, respectively. The pink line with a dot represents the position and the heading direction of the mobile robot at a specific time t_i in light blue

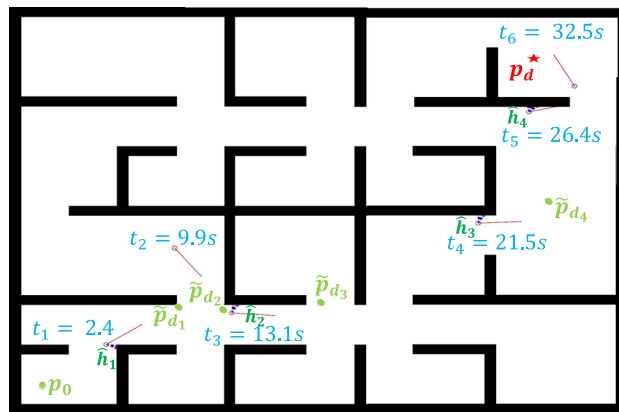


Table 3 The parameter settings of the indoor scenario

Initial values	$p_0 = [2, 2]^T, v_0 = [0, 0]^T, T = 10 \text{ Hz}$
Target values	$p_d = [22, 18]^T, v_d = [0, 0]^T$
IL-CBF	$\Phi = [1, x, x^2], S_\theta = [-\pi/2, \pi/2], S_r = 0.5 \text{ m}$
GD-CLF	$P = \begin{bmatrix} 25 & 12.5 \\ 12.5 & 25 \end{bmatrix}, Q = \begin{bmatrix} 50 & 25 \\ 25 & 50 \end{bmatrix}$
QP and LP	$S_\theta = [-\pi, \pi], S_r = 4 \text{ m}, \bar{c}_2 = 1.5$ $\bar{u}_x, \bar{u}_y = 20, \bar{c}_1 = 1, \alpha(t_0) = [5, 6]^T, \bar{\alpha} = 6$

Fig. 9 The trajectories of position p , velocity v , motion command u , and optimized α^* for the indoor scenario

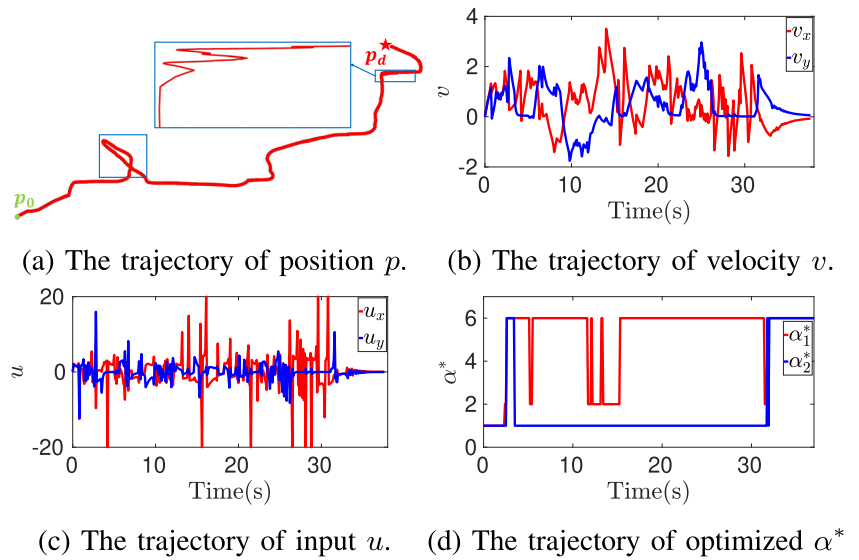


Fig. 10 The validation of the SFMP strategy in different simulated environments. The yellow cart uses a sensor with a limited detection range shown in blue to perceive the environment, wherein the cylinders denote the static obstacles, and the cuboids present the dynamic obstacles

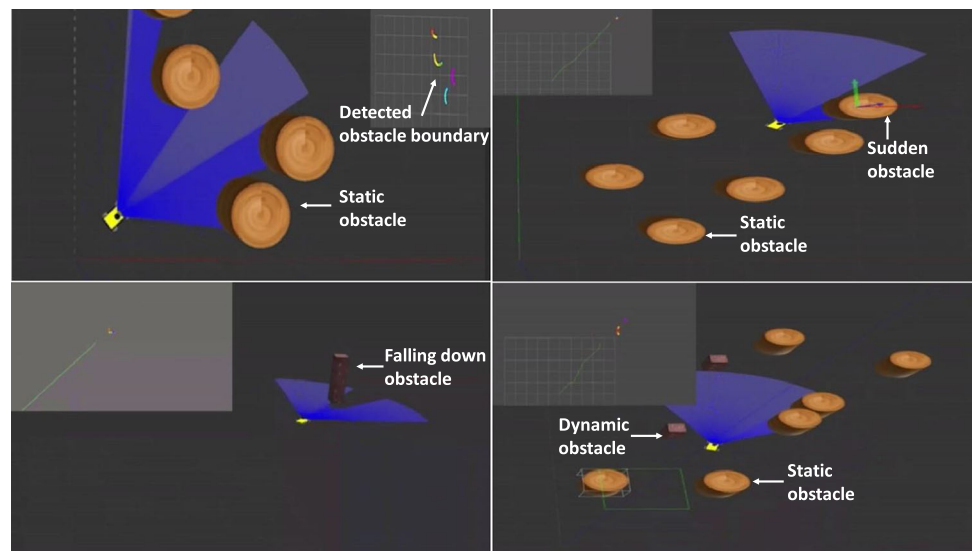
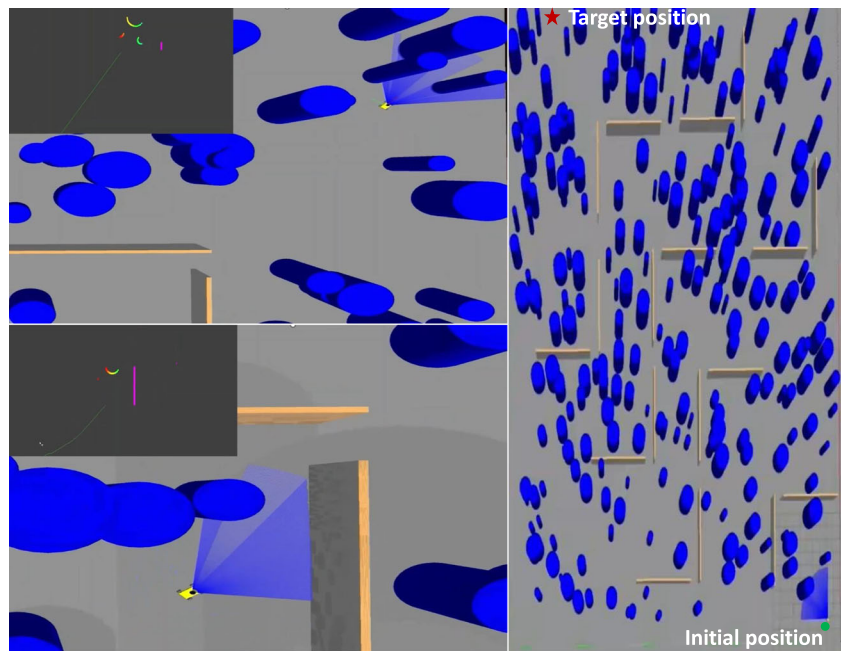


Fig. 11 The validation of the proposed SFMP strategy in a large environment. The map size is 50 m \times 50 m. Left: the screenshots of the mobile robot and the environment at specific time instants; Right: the top view of the task and the environment; The blue cylinders and brown walls denote obstacles; The green point and the red pentagram denote the initial and target positions, respectively



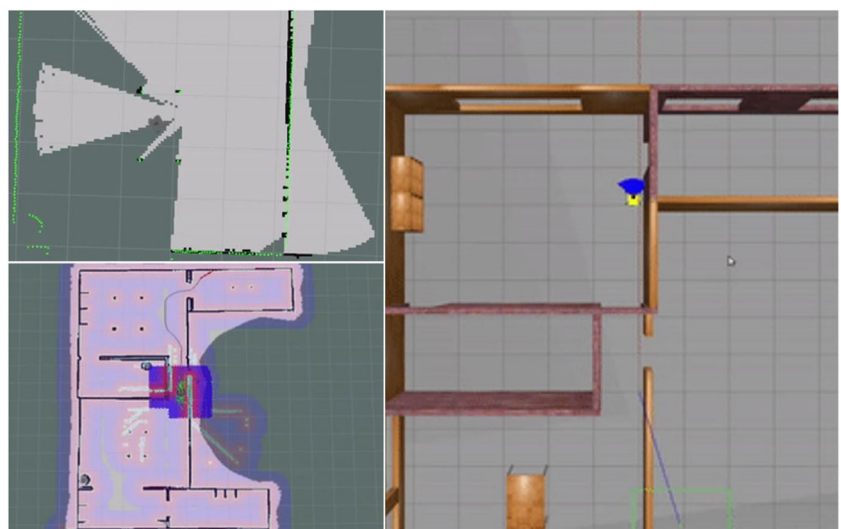
7.4 Validation in High-fidelity Simulator

We further evaluate the performance of our proposed SFMP strategy Eq. 9 in different scenarios based on Gazebo [36] and robot operating system (ROS) [37]. The simulations are conducted on the Ubuntu 18.04 computer with 16 GB RAM and 2.6-GHz Intel Core i7-9750H CPU. The adopted Mecanum wheel cart is equipped with a LiDAR sensor ($S_\theta = [-\pi/4, \pi/4]$, $S_r = 4$ m) to perceive the surrounding environment. To account for the robot volume's influence on safety, the original detected obstacle boundary samples are projected backwards along the LiDAR laser line by a distance $d = 0.5$ m.

7.4.1 Basic Demos

The effectiveness of our developed SFMP strategy Eq. 9 for the safe operation in unknown environments is validated via the following purposely designed cases: (a) static obstacles (the top-left Fig. 10); (b) static plus suddenly added static obstacles (the top-right Fig. 10); (c) falling down dynamic obstacles (the bottom-left Fig. 10); and (d) static plus dynamic obstacles (the bottom-right Fig. 10). Note that we simply extend the learned IL-CBFs Eq. 7 to avoid collision with dynamic obstacles here. Although without rigorous analysis, we found that the learned IL-CBFs could also address slowly moving obstacles. This is because

Fig. 12 The comparative evaluations conducted in a room in the size 12 m \times 16 m. The left figures are snapshots related to the baseline RRT method. Top left: the time-consuming mapping process; Bottom left: the movement of the cart on a pre-built map. The right figure is a snapshot of the movement of the cart driven by our method



we use instantaneous sensory data (reflecting the environmental changes timely) for collision avoidance. The results shown in Fig. 10 and the associated video at https://youtu.be/bpWW9R_MYpc validate that our proposed SFMP strategy Eq. 9 would drive the cart to survive in these four first-entry environments populated with static and dynamic obstacles.

7.4.2 Large Environment

We further examine the performance of the SFMP strategy Eq. 9 in a large environment (a mix of outdoor and indoor scenarios), see Fig. 11 and the associated video in <https://youtu.be/hDdyKatrCA>. We randomly sample 10 initial positions in the circle with center $c_0 = (0, 0)$ and radius $r_0 = 5\text{ m}$, and 10 goal positions in the circle with center $c_t = (45, 45)$ and radius $r_t = 5\text{ m}$. The proposed SFMP strategy succeeds 9 times out of 10. The success to survive in this complex environment without collisions and finally reaching the target position proves the practicability of our method regarding the robustness towards varying tasks (represented as different initial and target positions). Note that we purposely use the bottom-left initial position and the top-right target position in Fig. 10 to simulate a long-horizon task and also encourage the mobile robot to meet more obstacles.

7.4.3 Comparative Evaluation

This part focuses on the safe execution task in a room to show the superiority of our SFMP strategy Eq. 9 over the baseline rapidly exploring random tree (RRT) method [38] (a common sampling-based motion planning strategy) in terms of time. A supplementary video is referred to in https://youtu.be/lelW7C_mfsE. For the scenario displayed in Fig. 12, the common approach used in [38] would firstly build a perfect map using the SLAM technique (1025 seconds in the top-left Fig. 12) and then RRT generates a collision-free path followed by a PD controller (70 seconds in the bottom-left Fig. 12). In summary, the common approach would consume 1025 seconds in total to generate a safe solution in this room scenario. Our developed approach (the right Fig. 12) perceives the local environment and outputs the SFMP strategy Eq. 9 that drives the cart from the initial position to the target position. The utilized total time is 114 seconds. Regarding the first-entry environment, especially with no need to build a perfect global map, our SFMP strategy Eq. 9 enjoys an obvious advantage regarding time.

8 Conclusion

This work presents a safe feedback motion planning strategy that fulfills the nontrivial safe operation in prior-unknown environments. Our developed instantaneous local control

barrier functions are united with goal-driven control Lyapunov functions in a quadratic programming optimization framework to generate safe feedback motion planning strategies. The formulated linear programming optimization enhances the quadratic programming solution feasibility by enlarging the admissible control spaces of instantaneous local control barrier functions. Multiple conducted numerical validations fully prove the effectiveness of our proposed safe feedback motion planning strategy. The future work aims to extend our developed instantaneous local control barrier functions to realize collision avoidance with dynamic obstacles within consideration of obstacles' velocity and size. Besides, fully exploiting the maneuverability of the mobile robot to reach the target position in a time-optimal way is well worth investigating.

Author Contributions Cong Li contributed to the first draft of the manuscript and the development of the theoretical contributions. Zengjie Zhang contributed to the analysis and interpretation of the results. Nesrin Ahmed contributed to implementing the numerical validations. Qingchen Liu, Fangzhou Liu and Martin Buss supervised the study design, and reviewed, edited, and prepared the final version of the paper.

Funding This work was supported in part by the National Natural Science Foundation of China under Grant 62373123, and in part by the Fundamental Research Funds for the Central Universities under Grant WK2100000035.

Data Availability Data and materials used are available by contacting the corresponding author.

Code Availability The complete simulation data is available by contacting the corresponding author.

Declarations

Ethics Approval Not applicable.

Consent to Participate Not applicable.

Consent for Publication All authors have approved and consented to publish the manuscript.

Conflict of Interests The authors have no relevant financial or non-financial interests to disclose.

Open Access This article is licensed under a Creative Commons Attribution 4.0 International License, which permits use, sharing, adaptation, distribution and reproduction in any medium or format, as long as you give appropriate credit to the original author(s) and the source, provide a link to the Creative Commons licence, and indicate if changes were made. The images or other third party material in this article are included in the article's Creative Commons licence, unless indicated otherwise in a credit line to the material. If material is not included in the article's Creative Commons licence and your intended use is not permitted by statutory regulation or exceeds the permitted use, you will need to obtain permission directly from the copyright holder. To view a copy of this licence, visit <http://creativecommons.org/licenses/by/4.0/>.

References

- Hudson, N., Talbot, F., Cox, M., Williams, J., Hines, T., Pitt, A., Wood, B., Frousheger, D., Surdo, K.L., Molnar, T., et al.: "Heterogeneous ground and air platforms, homogeneous sensing: Team csiro data61's approach to the darpa subterranean challenge." Preprint at [arXiv:2104.09053](https://arxiv.org/abs/2104.09053) (2021)
- LaValle, S.M.: Planning algorithms. Cambridge university press (2006)
- Jaffar, M.K.M., Otte, M.: "Pip-x: Funnel-based online feedback motion planning/replanning in dynamic environments." In: International Workshop on the Algorithmic Foundations of Robotics. Springer, pp. 132–148 (2022)
- Majumdar, A., Tedrake, R.: Funnel libraries for real-time robust feedback motion planning. *Int. J. Robot. Res.* **36**(8), 947–982 (2017)
- Reist, P., Preiswerk, P., Tedrake, R.: Feedback-motion-planning with simulation-based lqr-trees. *Int. J. Robot. Res.* **35**(11), 1393–1416 (2016)
- Yershov, D.S., Frazzoli, E.: Asymptotically optimal feedback planning using a numerical hamilton-jacobi-bellman solver and an adaptive mesh refinement. *Int. J. Robot. Res.* **35**(5), 565–584 (2016)
- Agha-Mohammadi, A.-A., Chakravorty, S., Amato, N.M.: Firm: Sampling-based feedback motion-planning under motion uncertainty and imperfect measurements. *Int. J. Robot. Res.* **33**(2), 268–304 (2014)
- Lavalle, S.M., Konkimalla, P.: Algorithms for computing numerical optimal feedback motion strategies. *Int. J. Robot. Res.* **20**(9), 729–752 (2001)
- Claussmann, L., Revilloud, M., Gruyer, D., Glaser, S.: A review of motion planning for highway autonomous driving. *IEEE Trans. Intell. Transp. Syst.* **21**(5), 1826–1848 (2019)
- LaValle, S.M., Kuffner, J.J.: "Rapidly-exploring random trees: Progress and prospects: Steven m. lavalle, iowa state university, a james j. kuffner, jr., university of tokyo, tokyo, japan." *Algorithmic and computational robotics*, pp. 303–307 (2001)
- Tordesillas, J., Lopez, B.T., Everett, M., How, J.P.: Faster: Fast and safe trajectory planner for navigation in unknown environments. *IEEE Trans. Robot.* **38**(2), 922–938 (2021)
- Rimon, E., Koditschek, D.E.: "Exact robot navigation using artificial potential functions." *Departmental Papers (ESE)* (1992)
- Sunkara, V., Chakravarthy, A., Ghose, D.: Collision avoidance of arbitrarily shaped deforming objects using collision cones. *IEEE Robot. Autom. Lett.* **4**(2), 2156–2163 (2019)
- Tanner, H.G., Boddu, A.: Multiagent navigation functions revisited. *IEEE Trans. Robot.* **28**(6), 1346–1359 (2012)
- Mitchell, I.M., Bayen, A.M., Tomlin, C.J.: A time-dependent hamilton-jacobi formulation of reachable sets for continuous dynamic games. *IEEE Trans. Autom. Control* **50**(7), 947–957 (2005)
- Ames, A.D., Xu, X., Grizzle, J.W., Tabuada, P.: Control barrier function based quadratic programs for safety critical systems. *IEEE Trans. Autom. Control* **62**(8), 3861–3876 (2016)
- Zhao, H., Zeng, X., Chen, T., Liu, Z.: "Synthesizing barrier certificates using neural networks." In: Proceedings of the 23rd International Conference on Hybrid Systems: Computation and Control, pp. 1–11 (2020)
- Jin, W., Wang, Z., Yang, Z., Mou, S.: "Neural certificates for safe control policies." Preprint at [arXiv:2006.08465](https://arxiv.org/abs/2006.08465) (2020)
- Jagtap, P., Pappas, G.J., Zamani, M.: "Control barrier functions for unknown nonlinear systems using gaussian processes." In: 2020 59th IEEE Conference on Decision and Control (CDC), pp. 3699–3704 (2020)
- Saveriano, M., Lee, D.: "Learning barrier functions for constrained motion planning with dynamical systems." In: 2019 IEEE/RSJ International Conference on Intelligent Robots and System (IROS), pp. 112–119 (2019)
- Robey, A., Hu, H., Lindemann, L., Zhang, H., Dimarogonas, D.V., Tu, S., Matni, N.: "Learning control barrier functions from expert demonstrations." In: 2020 59th IEEE Conference on Decision and Control (CDC), pp. 3717–3724 (2020)
- Srinivasan, M., Dabholkar, A., Coogan, S., Vela, P.A.: Synthesis of control barrier functions using a supervised machine learning approach. In: 2020 IEEE/RSJ International Conference on Intelligent Robots and Systems (IROS), pp. 7139–7145 (2020)
- Freeman, R.A.: Robust control of nonlinear systems. University of California, Santa Barbara (1995)
- Abate, A., Ahmed, D., Giacobbe, M., Peruffo, A.: Formal synthesis of lyapunov neural networks. *IEEE Control Syst. Lett.* **5**(3), 773–778 (2020)
- Capelli, B., Secchi, C., Sabatini, L.: "Passivity and control barrier functions: Optimizing the use of energy." *IEEE Robot. Autom. Lett.* (2022)
- Xiao, W., Belta, C.: High-order control barrier functions. *IEEE Trans. Autom. Control* **67**(7), 3655–3662 (2021)
- Xu, X.: Constrained control of input-output linearizable systems using control sharing barrier functions. *Automatica* **87**, 195–201 (2018)
- Grammatico, S., Blanchini, F., Caiti, A.: Control-sharing and merging control lyapunov functions. *IEEE Trans. Autom. Control* **59**(1), 107–119 (2013)
- Xiao, W., Cassandras, G.C., Belta, C.: Safety-critical optimal control for autonomous systems. *J. Syst. Sci. Complex.* **34**(5), 1723–1742 (2021)
- Ester, M., Krieger, H.-P., Sander, J., Xu, X., et al.: A density-based algorithm for discovering clusters in large spatial databases with noise. *Kdd*, vol. 96, no. 34, pp. 226–231 (1996)
- Rawlings, J.O., Pantula, S.G., Dickey, D.A.: *Applied regression analysis: a research tool*. Springer Science & Business Media (2001)
- Holland, P.W., Welsch, R.E.: Robust regression using iteratively reweighted least-squares. *Commun. Stat. - Theory Methods.* **6**(9), 813–827 (1977)
- Xiao, W., Cassandras, C.G., Belta, C.A., Rus, D.: "Control barrier functions for systems with multiple control inputs." In: American Control Conference (ACC). IEEE, 2221–2226 (2022)
- Team, M.S.C.: "Mobile robotics simulation toolbox." [Online]. Available: <https://github.com/mathworks-robotics/mobile-robotics-simulation-toolbox> (2023)
- Coleman, T., Branch, M.A., Grace, A.: "Optimization toolbox." (1999)
- Koenig, N., Howard, A.: "Design and use paradigms for gazebo, an open-source multi-robot simulator." In: 2004 IEEE/RSJ International Conference on Intelligent Robots and Systems (IROS)(IEEE Cat. No. 04CH37566), vol. 3, pp. 2149–2154. IEEE (2004)
- Quigley, M., Conley, K., Gerkey, B., Faust, J., Foote, T., Leibs, J., Wheeler, R., Ng, A.Y., et al.: "Ros: an open-source robot operating system." In: ICRA workshop on open source software, vol. 3, no. 3.2, p. 5. Kobe, Japan (2009)
- Fazil, M.: Ros autonomous slam using rapidly exploring random tree (rtt). [Online]. Available: https://github.com/fazildgr8/ros_autonomous_slam (2021)

Publisher's Note Springer Nature remains neutral with regard to jurisdictional claims in published maps and institutional affiliations.

Cong Li received the Ph.D. degree in learning-based control and robotics with the Chair of Automatic Control Engineering, Technical University of Munich, Munich, Germany, in 2022. He was a Research Associate with the Chair of Automatic Control Engineering, Technical University of Munich. He is currently a Postdoc with the College of Intelligence Science and Technology, National University of Defense Technology, Changsha, China. His research interests include reinforcement learning, optimal control, robust control, constraint optimization, and robotics.

Zengjie Zhang received his Bachelor and Master degrees from Harbin Institute of Technology, China, in 2013 and 2015 respectively. He received the Doktor-Ingenieur degree in electrical engineering from the Technical University of Munich, Germany, in 2020. He was a Research Associate at the Chair of Automatic Control Engineering of the Technical University of Munich, Germany while pursuing the doctoral degree. Now he is within the Department of Electrical Engineering, Eindhoven University of Technology, The Netherlands. His research interests include sliding mode control, fault detection and isolation and human-robot collaboration.


Nesrin Ahmed received his Bachelor and Master degrees from Technical University of Munich, Germany, in 2017 and 2020 respectively. Her interests include optimal control and collision avoidance.

Qingchen Liu received the Ph.D degree in system and control from the Australian National University, Canberra, Australia, in 2018. From 2018 to 2019, he worked as a Postdoc Research Fellow in the same group. From 2019-2021, he was an EuroTech Research Fellow at the Chair of Information-Oriented Control, Technical University of Munich, Munich, Germany. He is now a Research Associate Professor at the Department of Automation, University of Science and Technology of China. His research interest includes networked systems and multi-robotics systems.

Fangzhou Liu received the M.Sc. degree in control theory and engineering from Harbin Institute of Technology, Harbin, China, in 2014, and the Doktor-Ingenieur degree in electrical engineering from the Technical University of Munich, Germany, in 2019. He was a Lecturer and a Research Fellow with the Chair of Automatic Control Engineering, Technical University of Munich, Munich, Germany. He is currently a Full Professor at the School of Astronautics, Harbin Institute of Technology. His research interests include networked control systems, modeling, analysis, and control on social networks, reinforcement learning and their applications. Dr. Liu has received the Dimitris N. Chorafas Prize and the Promotionspreis der Fakultät für Elektrotechnik und Informationstechnik.

Martin Buss received the Diploma Engineering degree in electrical engineering from the Technische Universität Darmstadt, Darmstadt, Germany, in 1990, and the Doctor of Engineering degree in electrical engineering from The University of Tokyo, Tokyo, Japan, in 1994. In 1988, he was a Research Student for one year with the Science University of Tokyo. From 1994 to 1995, he was a Post-Doctoral Researcher with the Department of Systems Engineering, The Australian National University, Canberra, ACT, Australia. From 1995 to 2000, he was a Senior Research Assistant and a Lecturer with the Chair of Automatic Control Engineering, Department of Electrical Engineering and Information Technology, Technical University of Munich, Munich, Germany. From 2000 to 2003, he was a Full Professor, the Head of the Control Systems Group, and the Deputy Director of the Faculty IV, Electrical Engineering and Computer Science, Institute of Energy and Automation Technology, Technical University of Berlin, Berlin, Germany. Since 2003, he has been a Full Professor (Chair) with the Chair of Automatic Control Engineering, Faculty of Electrical Engineering and Information Technology, Technical University of Munich, where he has been with the Medical Faculty since 2008. His research interests include automatic control, mechatronics, multimodal human system interfaces, optimization, nonlinear, and hybrid discrete-continuous systems.

Authors and Affiliations

Cong Li¹ · Zengjie Zhang²  · Nesrin Ahmed¹ · Qingchen Liu³ · Fangzhou Liu⁴ · Martin Buss¹

Cong Li
cong.lea@hotmail.com

Nesrin Ahmed
n.ahmed@tum.de

Qingchen Liu
qingchen_liu@ustc.edu.cn

Fangzhou Liu
fangzhouliu.ac@gmail.com

Martin Buss
mb@tum.de

¹ Chair of Automatic Control Engineering, Technical University of Munich, Theresienstr. 90, 80333 Munich, Germany

² Department of Electrical Engineering, Eindhoven University of Technology, 5600 MB, Eindhoven, The Netherlands

³ Department of Automation, University of Science and Technology of China, 230027 Hefei, China

⁴ Ningbo Institute of Intelligent Equipment Technology Company Ltd, 315000 Ningbo, China